Influence of alloying on the tensile strength and electrical resistivity of silver nanowire: copper composites macroscopic wires

Simon Tardieu, David Mesguich, Antoine Lonjon, Florence Lecouturier-Dupouy, Nelson Ferreira, Geoffroy Chevallier, Arnaud Proietti, Claude Estournès, Christophe Laurent

J Mater Sci (2021) 56:4884–4895

Metals & corrosion

Influence of alloying on the tensile strength and electrical resistivity of silver nanowire: copper composites macroscopic wires

Simon Tardieu[1,2], David Mesguich[1], Antoine Lonjon[1], Florence Lecouturier-Dupouy[2], Nelson Ferreira[2], Geoffroy Chevallier[1,3], Arnaud Proietti[4], Claude Estournès[1,3], and Christophe Laurent[1,*]

[1] CIRIMAT, CNRS-INPT-UPS, Université Toulouse 3 Paul-Sabatier, 118 Route de Narbonne, 31062 Toulouse Cedex 9, France
[2] Laboratoire National Des Champs Magnétiques Intenses, EMFL, CNRS-INSA-UGA-UPS, Grenoble, Toulouse, France
[3] Plateforme Nationale CNRS de Frittage Flash, PNF2, Université Toulouse 3 Paul-Sabatier, 118 route de Narbonne, Toulouse Cedex 9, MHT 31062, France
[4] Centre de Microcaractérisation Raimond Castaing, Université de Toulouse, UMS 3623, Espace Clément Ader, 3 rue Caroline Aigle, Toulouse 31400, France

Received: 7 July 2020
Accepted: 9 November 2020
Published online: 23 November 2020

ABSTRACT

Composite powders made up of 1 vol. %Ag nanowires (NW) dispersed in Cu were prepared and consolidated into cylinders by spark plasma sintering. One cylinder was sintered at only 400 °C resulting in a nanocomposite sample with no dissolution of the Ag NW into the Cu matrix. The second cylinder was sintered at 600 °C and the Ag NW are dissolved forming Ag/Cu alloy NW. The cylinders served as starting materials for room temperature wire-drawing, enabling the preparation of wires of decreasing diameters. The microstructure of the cylinders and the wires was investigated by electron microscopy and associated techniques. The tensile strength and electrical resistivity were measured at 293 K and 77 K. The nanocomposite and alloy wires show similar UTS values (1100 MPa at 77 K), but alloying, although spatially limited, provoked a significant increase in electrical resistivity (0.56 μΩ cm at 77 K) compared to the nanocomposite wires (0.49 μΩ cm at 77 K).

Handling Editor: P. Nash.

Address correspondence to E-mail: laurent@chimie.ups-tlse.fr

https://doi.org/10.1007/s10853-020-05556-9

GRAPHICAL ABSTRACT

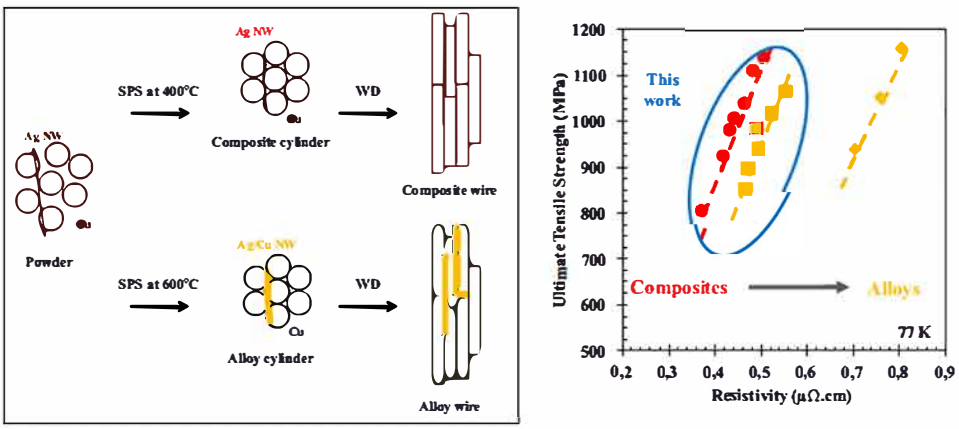

Introduction

Mechanically stronger electrically conducting wires are required in various domains such as record (100 T) pulsed magnetic fields, power and aerospace engineering. The requirements on electrical conductivity impose a material with a composition as close as possible to pure copper (Cu), therefore ruling out using metallic alloys [1]. Earlier studies have shown that nanocomposite Cu-matrix wires designed and prepared with a combination of ultrafine microstructure and one-dimensional (1D) reinforcement, such as carbon nanotubes (CNT) [2, 3] and silver nanowires (Ag NW) [4], show both a high ultimate tensile strength (UTS) and a low electrical resistivity. In particular, it has been established that Ag–Cu composite wires containing only 1 vol. % of Ag present the same UTS (1100 MPa at 77 K) than Ag/Cu alloy wires containing about 20 times more Ag [5–8] but with an electrical resistivity about 40% lower (0.51 μΩ cm vs 0.81 μΩ cm at 77 K). The ultrafine microstructure is obtained by the consolidation of a powder in the form of a cylinder by spark plasma sintering (SPS) followed by the room-temperature wire-drawing (WD) of the cylinders in wires of decreasing diameter. The method was first proposed and validated for pure Cu wires [9]. The short sintering times typical of SPS [10] avoid grain growth, producing Cu cylinders with micrometer-sized grains, 10 times smaller than for conventional cylinders. The extreme straining provoked by the multi-step WD process, a severe plastic deformation method [11–14], induces grain refinement down to ultrafine size (about 200–500 nm) and a high density of dislocations and point defects, leading to strengthening but also to a higher electrical resistivity. It is well known from general nanocomposites effect [15] that important gains may be achieved with very low proportion (typically 0.5–1 vol. %) of nanometer-sized compound dispersed in a matrix. Indeed, regarding the 1D reinforcement, this has been verified for the UTS of CNT-Cu [2, 3] and Ag NW-Cu [4] wires compared to that of pure Cu. It was highlighted that the use of such a low content of reinforcement is key to maintaining a low electrical resistivity of the wires. The aim of the present study is to bring to light some important differences between wires that are almost similar: 1 vol. % Ag–Cu composite wires will be prepared and compared to wires where Ag and Cu will not be present as separate phases anymore but rather will form an alloy. Both kind of wires will use the same powders, mixing process and WD process, but the composite cylinder will be sintered by SPS at 400 °C, where the solubility of Ag in Cu is below 0.1 vol. % Ag, whereas the alloy cylinder will be sintered at 600 °C, where the solubility of Ag in Cu is equal to about 2.4 vol. % Ag [16]. It is thus assumed that the Ag NW will not or only negligibly be dissolved at 400 °C and that they will be totally dissolved into the Cu grains at 600 °C, although the short time (5 min) at this temperature will not allow for the

diffusion of Ag over very long distances. In order to obtain an indication of the spatial extent of the resulting alloying for both temperatures, the diffusion length (L) of Ag in Cu during the SPS treatment was calculated according to Eq. (1):

$$L = \sqrt{D_{Ag\rightarrow Cu}t} \quad (1)$$

with L the diffusion length, $D_{Ag\rightarrow Cu}$ the lattice diffusion coefficient of Ag in Cu and t the duration. A value of $D_{Ag\rightarrow Cu}$ equal to 5.66 10^{-16} cm^2/s was used at 400 °C [17] and a value of $D_{Ag\rightarrow Cu}$ equal to 1.8 10^{-12} cm^2/s was used at 600 °C, according to a measurement at 595 °C [18].

Below 350 °C, the diffusion of Ag takes place along the Cu grain boundaries, but for higher temperatures, progressive dissolution takes place, corresponding to the so-called partial leakage of Ag from the Cu grain boundaries towards the interior of the Cu grains and therefore to the onset of some Ag diffusion in the Cu lattice [17]. It has also been shown [18] that the grain-boundary diffusion length is not distinguishable from the lattice diffusion length for misorientations lower than 20° or higher than 70° between the corresponding Cu grains. Therefore, we have used the lattice diffusion coefficient at 400 °C and 600 °C in Eq. (1) and neglected the grain boundary diffusion. Considering the length (30–60 μm) and diameter (200–300 nm) of the Ag NW, this corresponds to considering only a radial diffusion, neglecting that some Ag will indeed diffuse along the grain boundaries of the micrometer-sized Cu grains. For a 5 min dwell, the calculated L values are equal to 4 nm at 400 °C and to 232 nm at 600 °C. The values are in line with the hypotheses that there is no dissolution at 400 °C, whereas the 600 °C treatment transforms the Ag NW into more diffuse areas, still cylindrical but about three times larger in diameter (thus about 650 nm), made up of a Ag/Cu alloy. A schematic representation of the method and the expected microstructures of the samples is presented in Fig. 1.

Experimental procedure

Powders mixing

Ag NW (length 30–60 μm, diameter 200–300 nm) were prepared by reducing $AgNO_3$ (Aldrich, 99.9999%) with ethylene glycol in the presence of poly (vinyl pyrrolidone) [19]. A commercial Cu powder (Alfa Aesar, 99%, 0.5–1.5 μm) was used. An Ag NW-Cu composite powder (1 vol. % Ag) was prepared by step-wise pouring the appropriate amount of Cu powder into the Ag NW suspension in ethanol under sonication. The dry composite powder was obtained after ethanol evaporation in a rotary evaporator (80 °C). The so-obtained powder was heated at 160 °C (heating rate 2.5 °C.min^{-1}, dwell time 1 h) in flowing H_2 (15 L/h) to reduce any copper oxide present at the surface of the Cu grains and also to obtain a cohesive, pre-sintered powder because this was found to be favorable for the subsequent consolidation. Two powder batches were prepared in the same experimental conditions as required for the study.

Spark plasma sintering and wire-drawing

The Ag–Cu powders were sintered by SPS (PNF^2 Toulouse, Dr. Sinter 2080, SPS Syntex Inc., Japan) according to a procedure described elsewhere [4]. The sample is heated at 25 °C.min^{-1} from room temperature to 350 °C and then at 50 °C.min^{-1} from 350 °C to the maximum temperature where a 5 min dwell is applied. A uniaxial pressure (25 MPa) is applied gradually during the first minute of the dwell and is maintained for 4 min. The Ag–Cu powders were sintered at 400 and 600 °C, respectively, in order to obtain cylinders with a different microstructure. Indeed, as mentioned above, the Ag solubility limit in Cu at 400 °C is below 0.1 vol. % and therefore a composite microstructure should be maintained while at 600 °C it increases about 2.4 vol. %, as a total dissolution of the Ag NW is expected [16].

The cylinders (diameter 8 mm and length 30 mm) are designated S400 and S600 hereafter. The cylinders were wire-drawn at room temperature through conical WC dies, in about 49 steps, to obtain wires with decreasing diameters down to 0.19 mm. Wire samples were typically 700 or 1500 mm long. The wires are designated according to the starting cylinder and their diameter: for example, wire S400-0.5 is a 0.5 mm wire drawn from cylinder S400.

Characterization

Powders were observed by field-emission gun scanning electron microscopy (FEG-SEM, JEOL JSM 6700F). The microstructure of cylinders and wires was investigated by electron backscattered diffraction

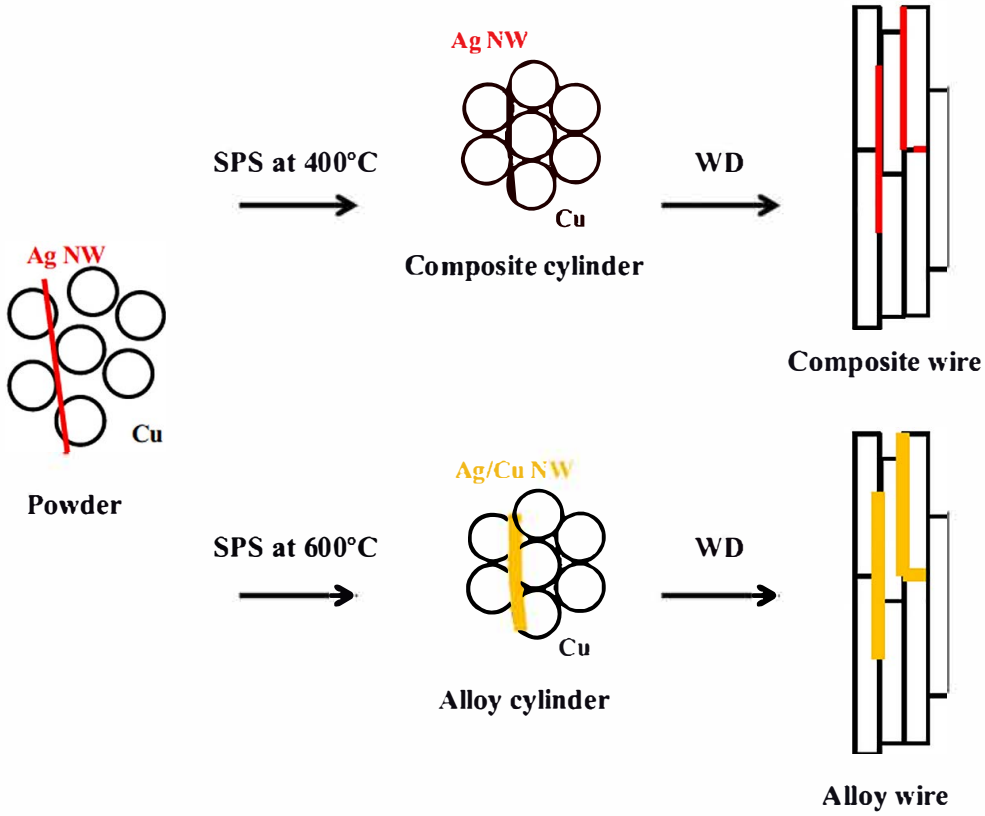

Figure 1 Schematic representation of the method and the expected microstructure and composition of the samples.

(EBSD) (NordlysNano, Oxford Instruments) combined with an energy dispersive X-ray spectrometry (EDS) (X-max 8080 mm^2, Oxford Instruments) on a FEG SEM JEOL JSM 7100F TTLS LV. Samples were prepared by ion milling, using a cross section polisher (JEOL IB-19510CP). The density was measured by Archimedes' method for the cylinder and the 4-mm-diameter wires. Microhardness was determined from indentation tests on polished surface in the transverse direction. Loading (1 N for 10 s at room temperature) was applied with a Vickers indenter (Shimadzu HMV M3). The distance between two successive indentations was 10 times the diagonal length of the indent and the reported microhardness values are the average of five tests or more. Tensile tests (INSTRON 1195 machine) were performed at 293 K and 77 K on 170-mm-long wires. Reported values are the average of three tests. Precise stresses were measured by the stress gauge system (1000 N or 250 N, 1.6×10^{-5} m s^{-1}). The error on the UTS determination is 2%. During the tensile test, it was not possible to follow the strain with an extensometer due to the small diameter of most wires and, in some cases, the testing itself being performed at 77 K. Strain was determined from crosshead displacement without any correction of the machine rigidity. The electrical resistivity of 350-mm-long wires was measured at 293 K and 77 K using the four-probe method with a maximum current of 100 mA to avoid heating the wires.

Results and discussion

Powders

A typical SEM image (Fig. 2a) of the Ag–Cu powder before the H_2 reduction step shows that the Ag NW are homogenously distributed among the spherical Cu particles. They do not appear to have been massively damaged during mixing, although some kinks and bends are observed along their length. The rough surface of the Cu grains (Fig. 2b) reveals the presence of copper oxide. After H_2 reduction, the Ag NW seem to be slightly more bent (Fig. 2c). The smooth surface of the Cu grains indicates the desired reduction of copper oxide in Cu. Sintering necks between adjacent

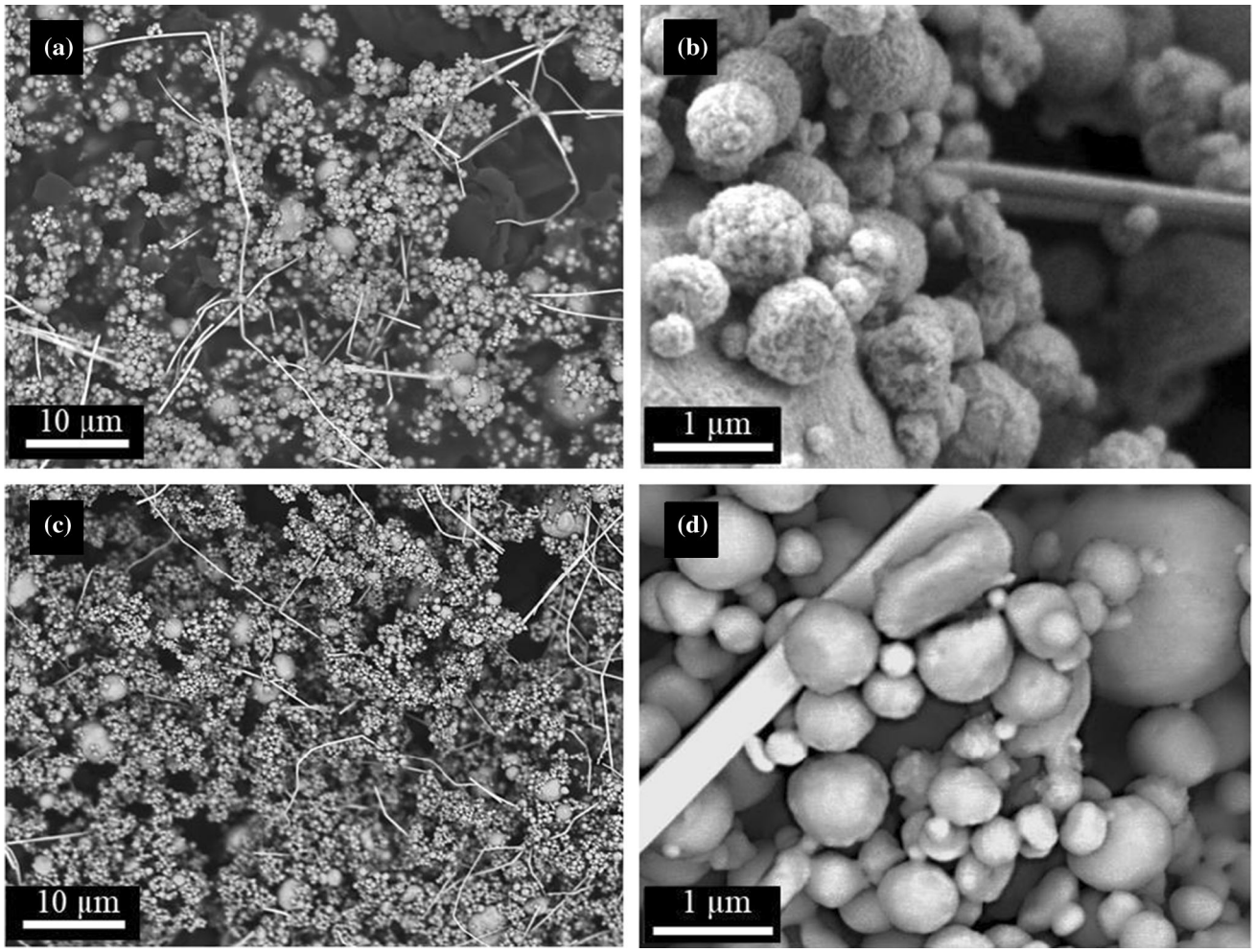

Figure 2 SEM images of the Ag Cu powder before (**a**, **b**) and after (**c**, **d**) the H_2 reduction step.

grains are observed, giving the powder some degree of cohesion (Fig. 2d).

Microstructure

The relative density of the cylinders is equal to 93 ± 1% for all samples. These values were found convenient for the rest of the study, because a too high density hampers the deformability of the cylinder during WD, resulting in sample breaking. Images of the transverse sections of S400 (Fig. 3a, b) and S600 (Fig. 3c, d) were recorded in back-scattered electrons mode to enhance the contrast between Ag (appearing white on the images) and Cu (grey). Black patches on the images reflect the presence of pores. The corresponding surface fraction is equal to 6.7% (Fig. 3a) and 5.4% (Fig. 3c) in acceptable agreement with the residual porosity (7 ± 1%) calculated from the Archimedes' method measurements. For S600 (Fig. 3c, d), it was not possible to distinguish shades of grey that would have indicated the presence and size of Ag-enriched areas, possibly because these areas are too diffuse. Moreover, the crystallographic contrasts are already very marked in back-scattered electrons mode. A 3D atom probe tomography analysis would be the best way to confirm our hypothesis.

EBSD analysis was performed in order to obtain the grain size distribution maps (Fig. 4).

Images of the transverse section of S400 (Fig. 3a, b and Fig. 4a) show that the Ag NW (d_{10} = 0.11 µm; d_{50} = 0.17 µm; d_{90} = 0.26 µm) are homogeneously dispersed in the Cu matrix made up of isotropic micrometric grains (Fig. 4a) (d_{10} = 0.40 µm; d_{50} = 0.91 µm; d_{90} = 1.88 µm) containing some annealing twins. This highlights the limited grain growth during sintering at 400 °C and confirm the expected composite microstructure. For S600, the Ag

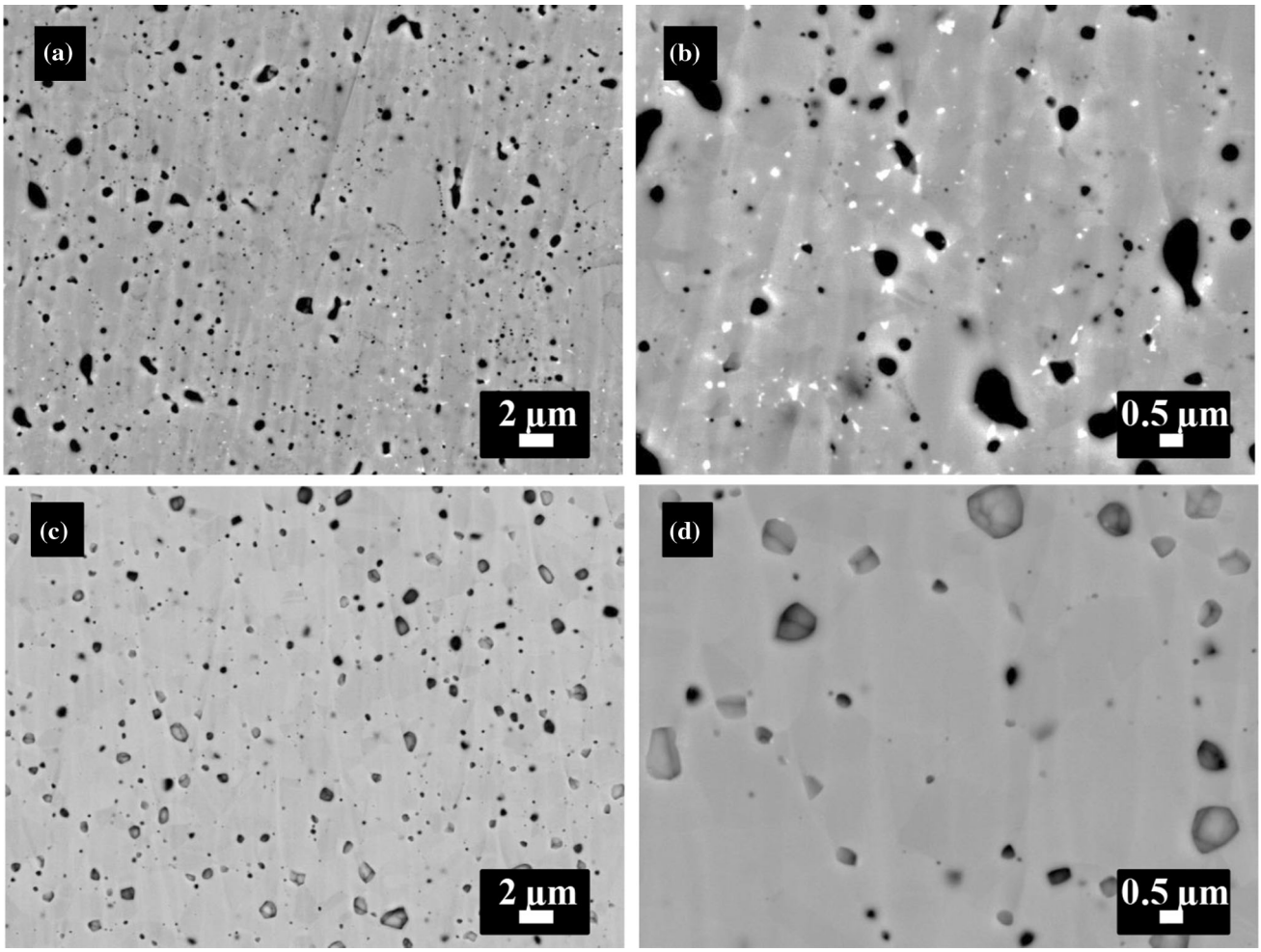

Figure 3 SEM images of transverse sections of the cylinders recorded in back scattered electrons mode: (**a**, **b**) S400 and (**c**, **d**) S600. Ag appears white on the images, Cu appears grey and pores appear black.

NW are no more observed on the SEM images (Fig. 3c, d) and the EBSD grain size distribution map (Fig. 4b) shows moderate increase of Cu grains size (d_{10} = 0.58 µm; d_{50} = 1.72 µm; d_{90} = 3.78 µm) in agreement with other studies [20]. The fcc Ag phase could not be detected anymore (i.e. any remaining free Ag is below the detection limit of SEM and EBSD) and the corresponding lack of observation of Ag NW as a discrete phase reflects their total dissolution into the Cu matrix despite the short sintering time (5 min) at 600 °C. This is in agreement with the hypotheses for the microstructure of the samples: there is negligible dissolution of the Ag NW at 400 °C and therefore S400 is a Ag–Cu composite made up of pure Ag and pure Cu, whereas S600 does not contain Ag NW anymore and is made up instead of localized Ag/Cu alloyed areas in the Cu matrix. Using the simple approximation, as mentioned above for the calculation of diffusion length, that the initial cylindrical Ag NW are uniformly dissolved into about three times larger NW, the Ag content of the so-obtained localized Ag/Cu alloy would be about 7 vol. %. Therefore, we propose to consider these localized areas as 7 vol. % Ag/Cu alloy NW with an average diameter of the order of 650 nm.

The diameter of the cylinders is reduced by WD at room temperature, forming progressively finer wires. The 4-mm-diameter wires are 99 ± 1% dense. The density is probably higher for lower-diameter wires but the measurement uncertainty is too high to give a meaningful value. Wire samples (1 mm down to 0.19 mm in diameter and 400 mm in length) are collected between WD passes in order to perform the microstructural, mechanical and electrical characterizations. It has been shown elsewhere [2–4, 9] that the CNT-Cu and Ag–Cu wires present the so-called

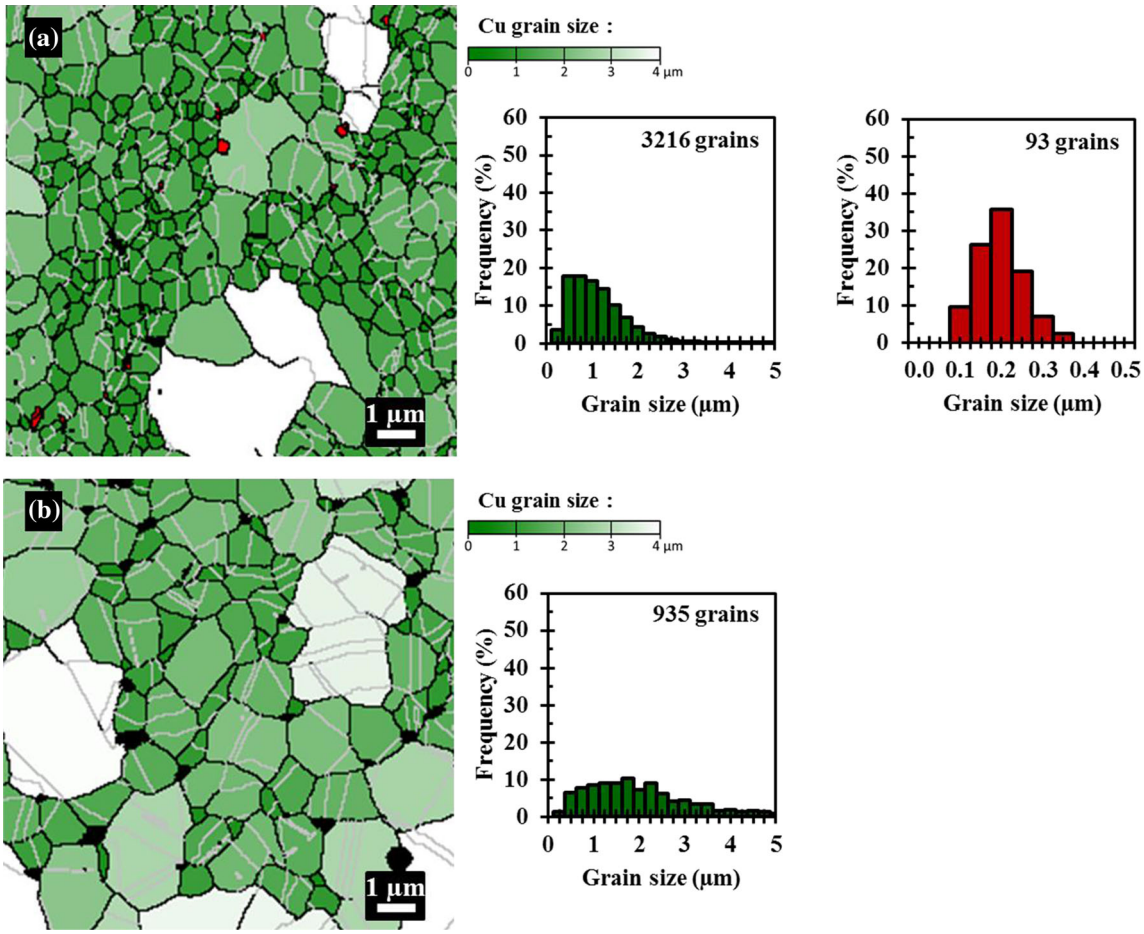

Figure 4 Grain size distribution maps obtained by EBSD of the transverse section and the corresponding Cu and Ag grain size distribution for the cylinder: **a** S400 and **b** S600. On the images, Ag is colored in red, Cu is colored in shades of green depending on the grain size, grain boundaries are colored in black, annealing twins are colored in grey and porosity is shown by black areas.

lamellar microstructure, with elongated grains parallel to the WD direction. The Cu grains are typically elongated over several micrometers with an average lamella width of the order of 0.28 µm for a CNT-Cu wire 0.5 mm in diameter [3] and in the range 0.2–0.4 µm for a 5 vol. % Ag–Cu wire 0.5 mm in diameter [4]. The Ag NW are dispersed along the Cu grain boundaries [4]. Coherent twin boundaries were not observed, by contrast to studies made on cryo-drawn wires [21–23]. The EBSD grain size distribution maps of the transverse section of the present 0.5 mm wire is presented in Fig. 5. Ag NW are observed for S400-0.5 (Fig. 5a), whereas they are not for S600-0.5 (Fig. 5b). The observed Ag NW sections are ultrafine and with a relatively narrow distribution (d_{10} = 0.14 µm; d_{50} = 0.17 µm; d_{90} = 0.21 µm). For Cu grains, the difference in grain size (lamella width) between S400-0.5 (d_{10} = 0.14 µm; d_{50} = 0.20 µm; d_{90} = 0.32 µm) and S600-0.5 (d_{10} = 0.15 µm; d_{50} = 0.20 µm; d_{90} = 0.34 µm) is significantly less marked than for the respective cylinders (Table 1).

The Cu grain size distribution for S400-0.3 and S600-0.3 was also studied by EBSD (Table 1). For S400-0.3, the Cu grain size distribution is the almost exactly the same (d_{10} = 0.14 µm; d_{50} = 0.19 µm; d_{90} = 0.31 µm) than for S400-0.5. The same was observed for S600-0.3 (d_{10} = 0.14 µm; d_{50} = 0.20 µm; d_{90} = 0.34 µm) compared to S600-0.5. This saturation in the grain size decreases although the decrease in wire diameter could reflect that the theoretical minimum grain size of Cu was reached, which corresponds to the size of a dislocation cell (0.2 µm), as shown by the d_{50} values.

The inverse pole figure maps of a transverse section of S400 (Fig. 6a) does not reveal any preferential texture. By contrast, the S400-0.5 (Fig. 6b) and S400-

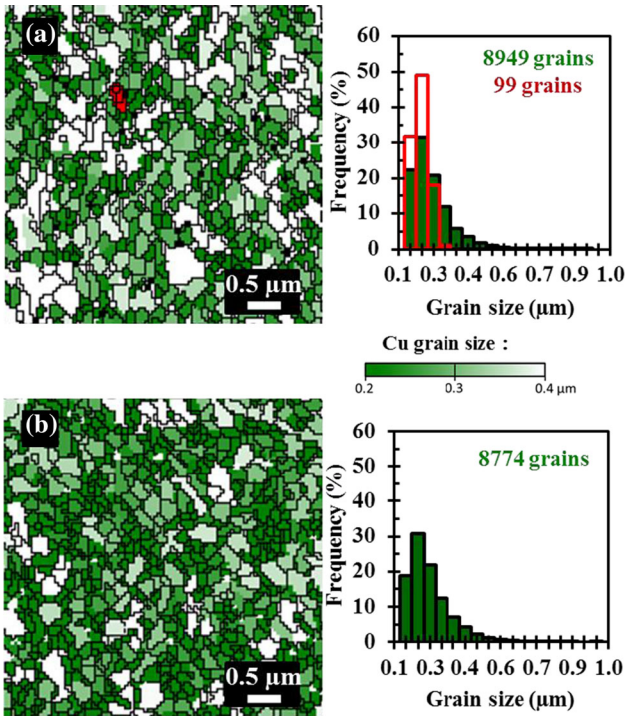

Figure 5 Grain size distribution maps obtained by EBSD and the corresponding Cu and Ag grain size distribution for the transverse section of the **a** S400 0.5 and **b** S600 0.5 wires. On the images, Ag is colored in red and Cu is colored in shades of green depending on the grain size.

0.3 (Fig. 6c) wires show < 111 > and < 100 > textures along the WD direction for both Ag and Cu, which are typical textures of face-centered cubic metals deformed by WD. For the S400-0.5 wire, the < 100 > and < 111 > orientations represent 79.5% and 16.5% of the image surface area, respectively, whereas for the S400-0.3, these values are equal to 85.4% and 11.2%, respectively. This shows that although the Cu grain size distribution has not been changed by WD from 0.5 to 0.3 mm, there are some differences between the wires.

Mechanical properties and electrical resistivity

The Vickers microhardness (Table 2) of the cylinders is equal to 120 and 75 HV for S400 and S600, respectively, reflecting the larger grain size for the latter as noted above. For the wires 4 mm in diameter, the values are slightly higher and they are still higher for the 1.0 mm and the 0.5 mm wires. This

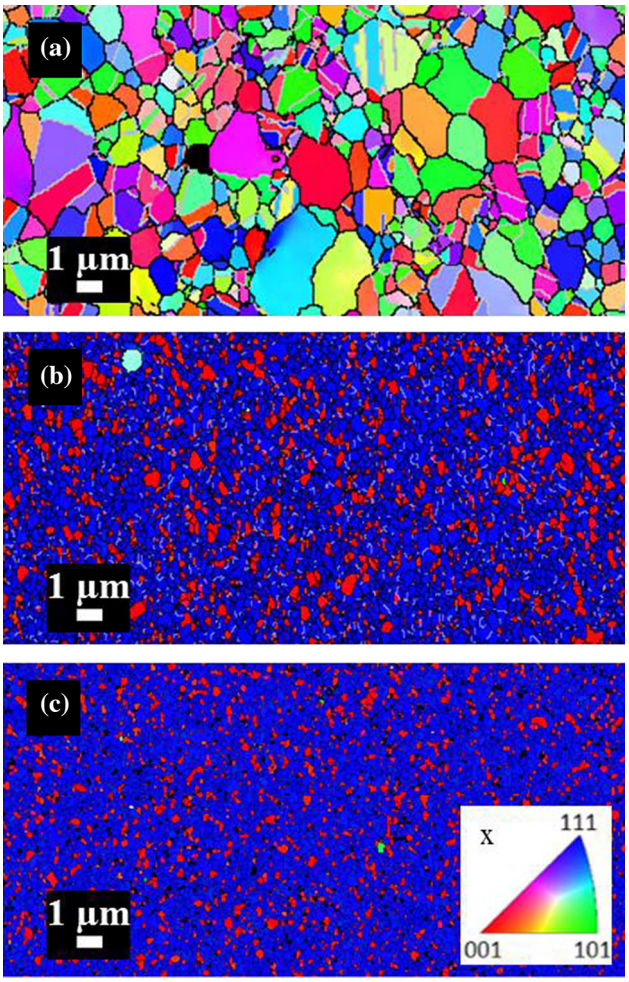

Figure 6 EBSD inverse pole figure maps along the drawing direction (X) of **a** the S400 cylinder, **b** the S400 0.5 wire and **c** the S400 0.3 wire.

Table 1 Cu grain size distribution for S400 and S600 for the SPS cylinder (diameter 8 mm) and the 0.5 and 0.3 mm wires

Sample	Diameter (mm)	d_{10} (µm)	d_{50} (µm)	d_{90} (µm)
S400	8	0.35	0.91	1.88
S400	0.5	0.14	0.20	0.32
S400	0.3	0.14	0.19	0.31
S600	8	0.58	1.72	3.78
S600	0.5	0.15	0.20	0.34
S600	0.3	0.14	0.20	0.34

could reflect the progressive densification and grain refinement, as reported elsewhere [4, 9].

Typical stress–strain curves for the 0.5 mm wires at 293 K and 77 K are shown in Fig. 7. The UTS values at 293 K (Fig. 8a) and 77 K (Fig. 8b) show an increase

Table 2 Vickers microhardness for S400 and S600 for the SPS cylinder (diameter 8 mm) and wires

Sample	Diameter (mm)	Microhardness ($Hv_{0.2}$)
S400	8	120
S400	4	131
S400	1	191
S400	0.5	193
S600	8	80
S600	1	172
S600	0.5	231

upon the decrease in wire diameter, which could reflect the refinement of the microstructure [2, 4]. For the pure Cu wires, earlier works [4, 9] have shown that strengthening originates from the propagation of dislocations by an Orowan-type dislocation glide mechanism in grains smaller than 250 nm. The Ag–Cu wires, regardless of the sintering temperature, show similar UTS values, in the ranges 700–900 MPa at 293 K (Fig. 8a) and 900–1150 MPa at 77 K (Fig. 8b). The latter higher values could reflect the lower mobility of the dislocations at 77 K. In all cases, the present values are significantly higher than those found elsewhere for pure Cu wires prepared from a cylinder sintered at 600 °C [4]. The Ag NW and the Ag/Cu alloy NW therefore appear to have the same effect on the mechanical reinforcement of the Ag–Cu wires. It is assumed that the Cu/Ag alloy NW present in the S600 cylinder due to the dissolution of the Ag NW have become thinner, elongated and oriented in the drawing direction during the WD just like the pure Ag NW have been. It is proposed that, similarly to what was observed for the Cu grains, the same grain size was reached in the Ag and Ag/Cu NW, despite the latter being larger prior to WD. This could show that the 1D-reinforcement effect is more dependent on the presence of the 1D second phase dispersed in the matrix than to its composition.

The electrical resistivity at 293 K and 77 K of all the samples is presented in Fig. 9. The electrical resistivity increases upon the decrease in wire diameter, because of the grain refinement and the increase in the density of grain boundaries acting as scattering centers for conduction electrons. It is in the range 1.93–2.02 μΩ cm (Fig. 9a) at 293 K for the S400 wires and slightly higher for the S600 wires. This moderate increase could reflect that the 293 K resistivity of the Cu grains still dominates as most of volume of the

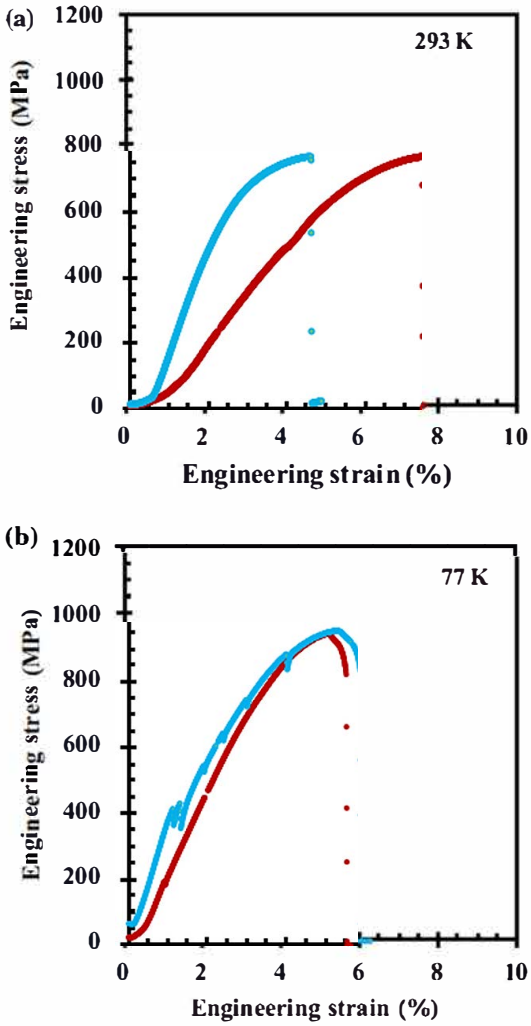

Figure 7 Stress strain curves t 293 K (a) and 77 K (b) for the 0.5 mm diameter wires: S400 0.5 ( ) and S600 0.5 ( ).

S600 wires is still pure Cu and the Ag/Cu alloy NW are highly localized around the position of the dissolved Ag NW. Indeed, the impact of Ag in solid solution in Cu on the increase in resistivity at room temperature, measured as 0.355 μΩ cm/wt. % Ag (i.e. 0.415 μΩ cm/vol. % Ag) [24] and 0.200 μΩ cm/wt. % Ag (i.e. 0.234 μΩ cm/vol. % Ag) [25], would have been significantly higher if the samples had uniformly been made up of a 1 vol. % Ag/Cu alloy. The electrical resistivity at 77 K is lower than at 293 K (Fig. 9b), reflecting the negligible electron–phonon interactions at low temperature. Interestingly, the electrical resistivity *vs* wire diameters curves of the S400 and S600 wires are roughly parallel to each other, higher for S600 (0.48–0.56 μΩ cm) than for S400 (0.380–51 μΩ cm). By contrast to what is observed for the UTS, this indicates a dramatic influence of the

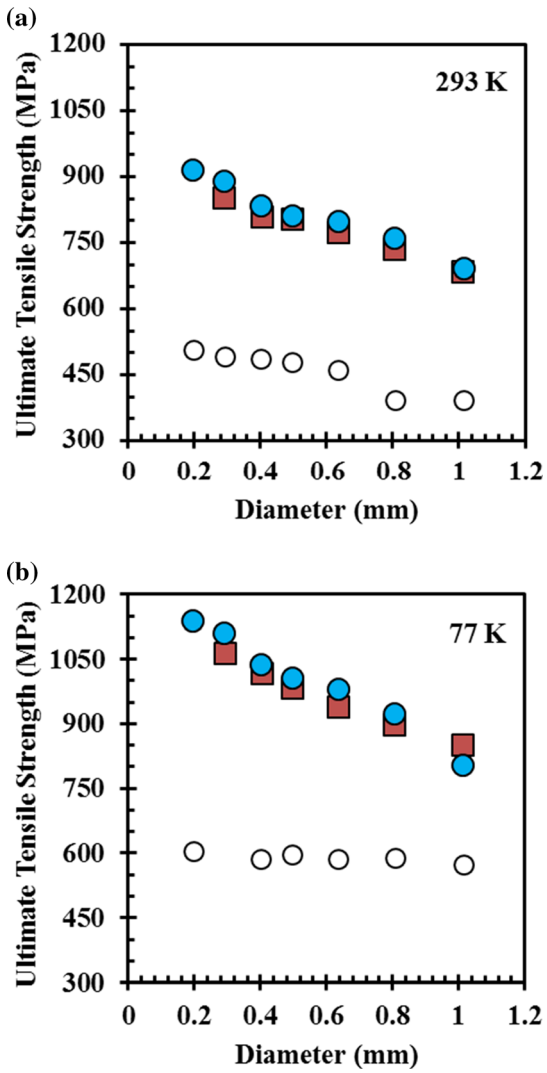

Figure 8 Ultimate tensile strength at **a** 293 K and **b** 77 K versus wire diameter for the wires prepared using Cu (black circle) [4] and the present S400 (blue circle) and S600 (brown square) cylinders. The error on the UTS measurement is 2%.

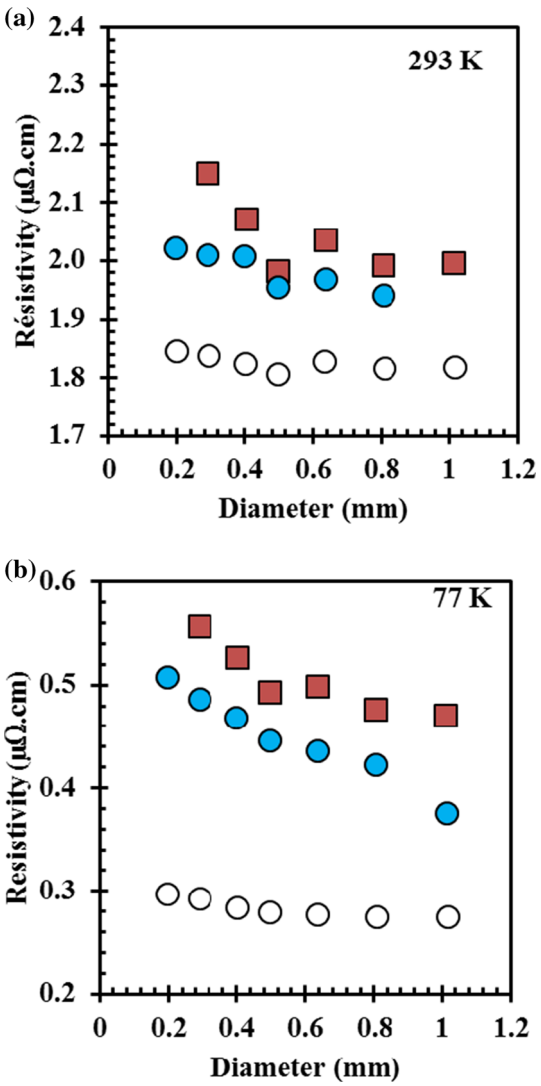

Figure 9 Electrical resistivity versus wire diameter at **a** 293 K and **b** 77 K for the wires prepared using Cu (black circle) [4] and the present S400 (blue circle) and S600 (brown square) cylinders.

dissolution of the Ag NW into Ag/Cu alloys NW upon sintering at 600 °C, although as noted above the increase could have been higher if the extent of the spatial dissolution of the Ag NW had been higher, due to the use of a higher SPS temperature or duration. The importance of this phenomenon is best seen on the UTS *vs* electrical resistivity plot (both at 77 K) presented in Fig. 10, notably when also compared to Ag/Cu alloy samples with higher Ag contents [6–8]. Note moreover that the latter samples were prepared by the melting-solidification route and therefore have a much more complex microstructure than the present powder-metallurgy samples.

Conclusions

Ag NW were mixed with a commercial Cu powder and the resulting powder (1 vol. % Ag) was divided in two batches for consolidation into cylinders by spark plasma sintering. One cylinder was sintered at only 400 °C and is a nanocomposite sample with no dissolution of the Ag nanowires. The second cylinder was sintered at 600 °C, a temperature high enough for the dissolution of the Ag NW, although it is spatially limited and results in the formation of Ag/Cu NW (7 vol. % Ag). Wires with ultrafine elongated Cu grains were prepared by room temperature wire-drawing of both cylinders. It is shown firstly that the

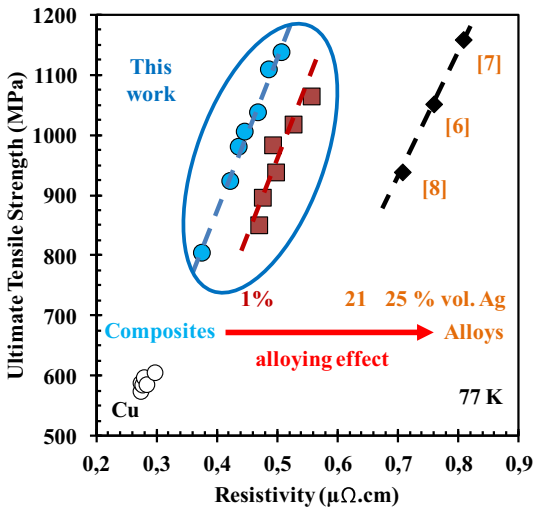

Figure 10 Ultimate tensile strength at 77 K versus electrical resistivity at 77 K for a selection of Cu (black circle) [4], the present S400 (blue circle) and S600 (blue square) wires and Cu/Ag alloy wires (21 25 vol. % Ag) (black diamond) [6 8]. Note that for [8] the UTS values were extrapolated at 77 K by adding 25 ± 5% to the room temperature values.

nanocomposite and alloy wires show similar UTS values (1100 MPa at 77 K), significantly higher than for pure Cu, reflecting an equivalent strengthening effect by the Ag NW and the Ag/Cu alloy NW located at the Cu grain boundaries. It is further shown that the alloying, although not widespread, did nevertheless provoke a small but significant increase in electrical resistivity compared to the nanocomposite wires. This evidences the need to obviate alloying during both the design and process of the wires and to remain as close as possible to pure Cu, relying only on low-loading nanocomposite effects for strengthening without compromising the electrical resistivity. These results could provide important guidelines for the design and preparation of ultra-strong yet electrically conducting macroscopic wires.

Acknowledgements

Electron microscopy was performed at "Centre de microcaractérisation Raimond Castaing—UMS 3623" (Toulouse). The authors thank Dr. C. Josse (Castaing), Dr. A. Weibel (CIRIMAT) and Dr. G. Rikken (LNCMI) for discussions.

Funding

This research did not receive any specific grant from funding agencies in the public, commercial, or not-for-profit sectors.

Data availability

The raw/processed data required to reproduce these findings cannot be shared at this time as the data also forms part of an ongoing study.

Compliance with ethical standards

Conflict of interest None

References

[1] Misra A, Thilly L (2010) Structural metals at extremes. MRS Bull 35:965 972. https://doi.org/10.1017/S0883769400100016

[2] Arnaud C, Lecouturier F, Mesguich D, Ferreira N, Chevallier G, Estournès C, Weibel A, Laurent C (2016) High strength high conductivity double walled carbon nanotube copper composite wires. Carbon 96:212 215. https://doi.org/10.1016/j.carbon.2015.09.061

[3] Mesguich D, Arnaud C, Lecouturier F, Ferreira N, Chevallier G, Estournès C, Weibel A, Josse C, Laurent C (2017) High strength high conductivity carbon nanotube copper wires with bimodal grain size distribution by spark plasma sintering and wire drawing. Scripta Mater 137:78 82. https://doi.org/10.1016/j.scriptamat.2017.05.008

[4] Tardieu S, Mesguich D, Lonjon A, Lecouturier F, Ferreira N, Chevallier G, Proietti A, Estournès C, Laurent C (2019) Nanostructured 1% silver copper composite wires with a high tensile strength and a high electrical conductivity. Mater Sci Eng A 761:138048. https://doi.org/10.1016/j.msea.2019.138048

[5] Sakai Y, Schneider Muntau HJ (1997) Ultra high strength, high conductivity Cu Ag alloy wires. Acta Mater 45:1017 1023. https://doi.org/10.1016/S1359 6454(96)00248 0

[6] Han K, Embury JD, Sims JR, Campbell LJ, Schneider Muntau HJ, Pantsyrnyi VI, Shikov A, Nikulin A, Vorobieva, (1999) A The fabrication, properties and microstructure of Cu Ag and Cu Nb composite conductors. Mater Sci Eng A 267:99 114. https://doi.org/10.1016/S0921 5093(99)00025 8

[7] Han K, Baca A, Coe H, Embury J, Kihara K, Lesch B, Li L, Schillig J, Sims J, Van Sciver S, Schneider Muntau HJ (2000) Material issues in the 100 T non destructive magnet. IEEE Trans Appl Supercond 10:1277 1280. https://doi.org/10.1109/77.828468

[8] Zuo X, Han K, Zhao C, Niu R, Wang E (2014) Microstructure and properties of nanostructured Cu 28 wt%Ag microcomposite deformed after solidifying under a high magnetic field. Mater Sci Eng A 619:319 327. https://doi.org/10.1016/j.msea.2014.09.070

[9] Arnaud C, Lecouturier F, Mesguich D, Ferreira N, Chevallier G, Estournès C, Weibel A, Peigney A, Laurent C (2016) High strength high conductivity nanostructured copper wires prepared by spark plasma sintering and room tem perature severe plastic deformation. Mater Sci Eng A 649:209 213. https://doi.org/10.1016/j.msea.2015.09.122

[10] Orru R, Licheri R, Locci AM, Cincotti A, Cao GC (2009) Consolidation/synthesis of materials by electric current activated/assisted sintering. Mater Sci Eng R 63:127 287. https://doi.org/10.1016/j.mser.2008.09.003

[11] Langdon TG (2013) Twenty five years of ultrafine grained materials: Achieving exceptional properties through grain refinement. Acta Mater 61:7035 7059. https://doi.org/10.1016/j.actamat.2013.08.018

[12] Estrin Y, Vinogradov A (2013) Extreme grain refinement by severe plastic deformation: a wealth of challenging science. Acta Mater 61:782 817. https://doi.org/10.1016/j.actamat.2012.10.038

[13] Raabe D, Choi PP, Li Y, Kostka A, Sauvage X, Lecouturier F, Hono K, Kirchheim R, Pippan R, Embury D (2010) Metallic composites processed via extreme deformation: toward the limits of strength in bulk materials. Mater Res Bull 35:982 991. https://doi.org/10.1557/mrs2010.703

[14] Hanazaki K, Shigeiri N, Tsuji N (2010) Change in microstructures and mechanical properties during deep wire drawing of copper. Mater Sci Eng A 527:5699 5707. https://doi.org/10.1016/j.msea.2010.05.057

[15] Laurent C, Rousset A (1995) Metal oxide ceramic matrix nanocomposites. Key Eng Mater 108 110:405 406. https://doi.org/10.4028/www.scientific.net/KEM.108 110.405

[16] Okamoto H, Schlesinger ME, Mueller EM (2016) ASM handbook vol. 3, alloy phase diagrams. ASM International, USA , pp 2 28

[17] Divinski S, Lohmann M, Herzig C (2001) Ag grain boundary diffusion and segregation in Cu: measurements in the types B and C diffusion regimes. Acta Mater 49:249 261. https://doi.org/10.1016/S1359 6454(00)00304 9

[18] Butrymowicz DB (1977) Diffusion rate data mass transport phenomena for copper systems. Inst. for Materials Research, National Bureau of Standards, Washington DC

[19] Lonjon A, Caffrey I, Carponcin D, Dantras E, Lacabanne C (2013) High electrically conductive composites of Poly amide 11 filled with silver nanowires: nanocomposites pro cessing, mechanical and electrical analysis. J Non Cryst Solids 376:199 204. https://doi.org/10.1016/j.jnoncrysol.2013.05.020

[20] Zhang ZH, Wang FC, Wang L, Li SK (2008) Ultrafine grained copper prepared by spark plasma sintering process. Mater Sci Eng A 476:201 205. https://doi.org/10.1016/j.msea.2007.04.107

[21] Lu L, Shen Y, Chen X, Qian L, Lu K (2004) Ultrahigh strength and high electrical conductivity in copper. Science 304:422 426. https://doi.org/10.1126/science.1092905

[22] Zhang BB, Tao NR, Lu K (2017) A high strength and high electrical conductivity bulk Cu Ag alloy strengthened with nanotwins. Scripta Mater 129:39 43. https://doi.org/10.1016/j.scriptamat.2016.10.022

[23] Kauffmann A, Freudenberger J, Klauß H, Klemm V, Schil linger W, Sarma VS, Schultz L (2013) Properties of cryo drawn copper with severely twinned microstructure. Mater Sci Eng A 588:132 141. https://doi.org/10.1016/j.msea.2013.09.022

[24] Davis JR (2001) ASM specialty handbook. ASM Interna tional, Copper and copper alloys, p 4

[25] Simon NJ (1992) Properties of copper and copper alloys at cryogenic temperatures. U.S. Dept. of Commerce, National Institute of Standards and Technology, Washington, D.C.